Hindawi Publishing Corporation
Journal of Nanomaterials
Volume 2016, Article ID 2463479, 9 pages
http://dx.doi.org/10.1155/2016/2463479

Research Article

Upconversion Luminescence and Magnetic Turning of $NaLuF_4:Yb^{3+}/Tm^{3+}/Gd^{3+}$ Nanoparticles and Their Application for Detecting Acriflavine

Shigang Hu,[1] Huiyi Cao,[1] Xiaofeng Wu,[1] Shiping Zhan,[2] Qingyang Wu,[1] Zhijun Tang,[1] and Yunxin Liu[2]

[1]*School of Information and Electrical Engineering, Hunan University of Science and Technology, Xiangtan 411201, China*
[2]*Department of Physics and Electronic Science, Hunan University of Science and Technology, Xiangtan 411201, China*

Correspondence should be addressed to Yunxin Liu; lyunxin@163.com

Received 17 September 2016; Accepted 12 October 2016

Academic Editor: Giovanni Bongiovanni

Fluorescent and magnetic bifunctional $NaLuF_4:Yb^{3+}/Tm^{3+}/Gd^{3+}$ nanocrystals were synthesized by the solvothermal method and subsequent surface modification. By changing the doping concentration of Gd^{3+}, the shape, size, luminescent properties, and magnetic properties of the nanoparticles can be modulated. These $NaLuF_4:Yb^{3+}/Tm^{3+}/Gd^{3+}$ nanocrystals present efficient blue upconversion fluorescence and excellent paramagnetic property at room temperature. Based on the luminescence resonance energy transfer (LRET), upconversion nanoparticles (UCNPs) were confirmed to be an efficient fluorescent nanoprobe for detecting acriflavine. It is easy to derive the concentration of acriflavine from the Integral Intensity Ratio of Green (emission from acriflavine) to Blue (emission from UCNPs) fluorescent signals. Based on this upconversion fluorescent nanoprobe, the detection limit of acriflavine can reach up to 0.32 μg/mL.

1. Introduction

Rare earth upconversion nanoparticles (UCNPs), which are able to emit high-energy photons under excitation by near-infrared (NIR) light, have three important features: the deep penetration of excitation light to the biotissues, the absence of background fluorescence in biological detection, and no obvious injury to biological tissues [1–5]. Thanks to various unique intrinsic properties, UCNPs have not only attracted growing attention in the biological chemistry, microarray applications, imaging, but also offered advantages for clinical applications in diagnosis and treatment [6–12]. Some recent study tuned UC emission through doping with Gd^{3+} ions [13–15]. Meanwhile, due to the large magnetic moment, the upconversion materials doped with Gd^{3+} can present excellent magnetic behavior. So bifunctional nanocrystals can be achieved by doping a suitable amount of Gd^{3+} ions.

Acriflavine is a typical antiseptic. It has the form of an orange or brown powder. It may be harmful in the eyes or if inhaled. It is a dye and it stains the skin and may irritate. Acriflavine is also used as treatment for external fungal infections of aquarium fish. In recent years, acriflavine has been confirmed to possess anticancer activity [16–18]. However, its potential clinical application is greatly undermined by its uncertain mechanism of activation. It is very important and valuable for detecting traces of acriflavine in vivo.

Fluorescence resonance energy transfer (FRET) is a nonradiative process in which the electronic excitation energy of a donor chromophore is transferred to a nearby acceptor molecule via long-range dipole-dipole interactions. Luminescence resonance energy transfer (LRET) is a specific FRET system with rare earth doped materials as the donor [19–21]. Recently LRET has been used to detect molecule binding events and protein [22–24]. Here, this LRET process based on upconversion fluorescent donors is developed for detecting organic dye acriflavine.

In this work, based on a simple Gd^{3+} doping method, shape and size of well controlled $NaLuF_4$ nanocrystals were

synthesized. The as-synthesized bifunctional $NaLuF_4$:Yb^{3+}/Tm^{3+}/Gd^{3+} nanocrystals with highly efficient UC luminescence and excellent paramagnetic behavior can be applied in many fields such as bioseparation, fluorescent, and MRI bioimaging. Here, an upconversion LRET system was applied to detect acriflavine.

2. Experimental

2.1. Materials. All rare earth oxides were of 99.99% purity. Rare earth chloride $RE(Cl)_3$ (RE = Lu, Yb, Tm, and Gd) solutions were prepared by dissolving the corresponding rare earth oxides in hydrochloric acid at a high temperature. All other chemicals were analytical grade and used without further purification.

2.2. Synthesis of $NaLuF_4$:Yb^{3+}/Tm^{3+}/Gd^{3+} Nanoparticles. Synthesis of $NaLuF_4$:Yb^{3+}/Tm^{3+}/Gd^{3+} nanoparticles was conducted according to a previously reported procedure as shown in [5, 11].

2.3. Characterization. The shape, size, and uniformity of synthesized UCNPs were measured with a transmission electron microscope (H-7650c) and a high-resolution transmission electron microscopy (JEM 3010). Upconversion luminescence spectra were recorded with a fluorescence spectrometer (Hitachi F-2700), which has a 980 nm laser as the excitation source. A multiple CCD camera (Sony) was used to take the pictures of the upconversion luminescence. Magnetic measurement of the $NaLuF_4$ microcrystals was made using a Lake-shore 7410 vibrating sample magnetometer. Animal tissue imaging with upconversion nanoparticles was conducted using Olympus BX43 fluorescence microscopy. All tests were performed at room temperature.

3. Results and Discussion

3.1. Upconversion Luminescence Properties of $NaLuF_4$:Yb^{3+}/Tm^{3+}/Gd^{3+} Nanoparticles. To reveal the phase and size control, $NaLuF_4$:Yb^{3+}/Tm^{3+}/Gd^{3+} nanocrystals synthesized by the solvothermal method were characterized by TEM and high-resolution TEM (HRTEM) as shown in Figure 1. The average diameters of the prepared $NaLuF_4$ nanoparticles doped with 20%Yb^{3+}/0.5%Tm^{3+}, 20%Yb^{3+}/0.5%Tm^{3+}/20%Gd^{3+}, and 20%Yb^{3+}/0.5%Tm^{3+}/60%Gd^{3+} are determined to be about 320, 180, and 20 nm, respectively. With the increase of Gd^{3+} content, particle size is gradually reduced. It can be observed from Figures 1(a) and 1(b) that $NaLuF_4$ nanoparticles doped with 20%Yb^{3+}/0.5%Tm^{3+} and 20%Yb^{3+}/0.5%Tm^{3+}/20%Gd^{3+} have typical hexagonal crystal facets and good crystallinity, while $NaLuF_4$:20%Yb^{3+}/0.5%Tm^{3+}/60%Gd^{3+} nanoparticles have a nanoplate morphology and uniform particle size as shown in Figure 1(c). All the three kinds of nanoparticles display regular morphology and good crystalline quality. From the high-resolution transmission electron microscopy (Figure 1(d)), it can be found that the distance between the lattice fringes is 0.31 nm along (0001) orientation in the $NaLuF_4$:20%Yb^{3+}/0.5%Tm^{3+}/60%Gd^{3+} nanocrystals, which also revealed their highly crystalline nature and structural uniformity.

Under the excitation of 980 nm infrared light, $NaLuF_4$:Yb^{3+}/Tm^{3+}/Gd^{3+} nanocrystals can emit intense blue light. As shown in Figure 2(a), five emission peaks in the ultraviolet-visible region were assigned to $^1I_6 \rightarrow {}^3F_4$ (344 nm), $^1D_2 \rightarrow {}^3H_6$ (361 nm), $^1D_2 \rightarrow {}^3F_4$ (450 nm), $^1G_4 \rightarrow {}^3H_6$ (476 nm), and $^1G_4 \rightarrow {}^3F_4$ (646 nm) transitions of the Tm^{3+} ions, respectively. With the increase of Gd^{3+} content, the UC emission intensity of $NaLuF_4$ samples increases first and then decreases evidently. When the concentration of Gd^{3+} ion reaches 20%, the luminescence intensity is the strongest. It can be seen from Figure 2(b) that the intensity ratios of the blue-to-UV emission and blue-to-red emission vary with the Gd^{3+} concentration. When the content of Gd^{3+} is equal to 10%, the blue-to-red ratio reaches the maximum value of 81.9 and the blue-to-UV ratio reaches the minimum value of 4.2.

Figure 3 shows the UC luminescence mechanism and population processes in an Yb^{3+}-Tm^{3+}-Gd^{3+} codoped system. With a 980 nm LD as the excitation source, Yb^{3+} successively transfers energy to Tm^{3+} to populate their levels. First, the Tm^{3+} ions are excited from the ground state $^3H_6$ to the excited state $^3H_5$ via the energy transfer (ET) from neighboring Yb^{3+} ions to the Tm^{3+} ions. Subsequent nonradiative relaxation of $^3H_5 \rightarrow {}^3F_4$ populates the $^3F_4$ level of Tm^{3+} ions. In the second-step excitation, Tm^{3+} ions in the $^3F_4$ state are excited to the $^3F_{2,3}$ states via the ET from excited Yb^{3+} ions. The populated $^3F_2$ level may nonradiatively relax to the $^3F_3$ and $^3H_4$ levels. The Tm^{3+} of $^3H_4$ state can absorb a third pump photon to an upper level $^1G_4$ level, which can yield red (646 nm) and blue (476 nm) emissions upon nonradiative relaxation back to $^3F_4$ and $^3H_6$ levels, respectively. There is another ET process from Yb^{3+} to Tm^{3+} ions which may take place to populate the Tm^{3+} from $^1G_4$ to $^1D_2$, which subsequently resulted in the ultraviolet (UV) and blue emission bands centered at 361 nm and 450 nm, respectively. On the other hand, the Tm^{3+} ions in the $^1D_2$ state can be excited to the $^1I_6$ state via another ET from excited Yb^{3+} ions. The UV emissions of ~344 nm can be observed simultaneously via the transitions of $^1I_6 \rightarrow {}^3F_4$, respectively. In addition, the strong ultraviolet emissions demonstrated the high upconversion efficiency in $NaLuF_4$:Yb^{3+}/Tm^{3+}/Gd^{3+} system since the successive absorption of three or more than three photons involved in the upconversion process of ultraviolet emissions. Some of Tm^{3+} ions in the $^3P_2$ state transfer energy to ^6I_J levels of Gd^{3+} through the ET $^3P_2 \rightarrow {}^3H_6$ (Tm^{3+}):$^8S_{7/2} \rightarrow {}^6I_J$ (Gd^{3+}) [25]. At room temperature, the nonradiative relaxation $^6I_J \rightarrow {}^6P_J$ leads to the population of $^6P_{5/2}$ and $^6P_{7/2}$ levels efficiently [26]. Then, the ^6D_J levels of Gd^{3+} can be populated further. Due to their appropriate energy matching, the ET $^2F_{5/2} \rightarrow {}^2F_{7/2}$ (Yb^{3+}):$^6P_{7/2} \rightarrow {}^6D_J$ (Gd^{3+}) should be the dominant process in populating

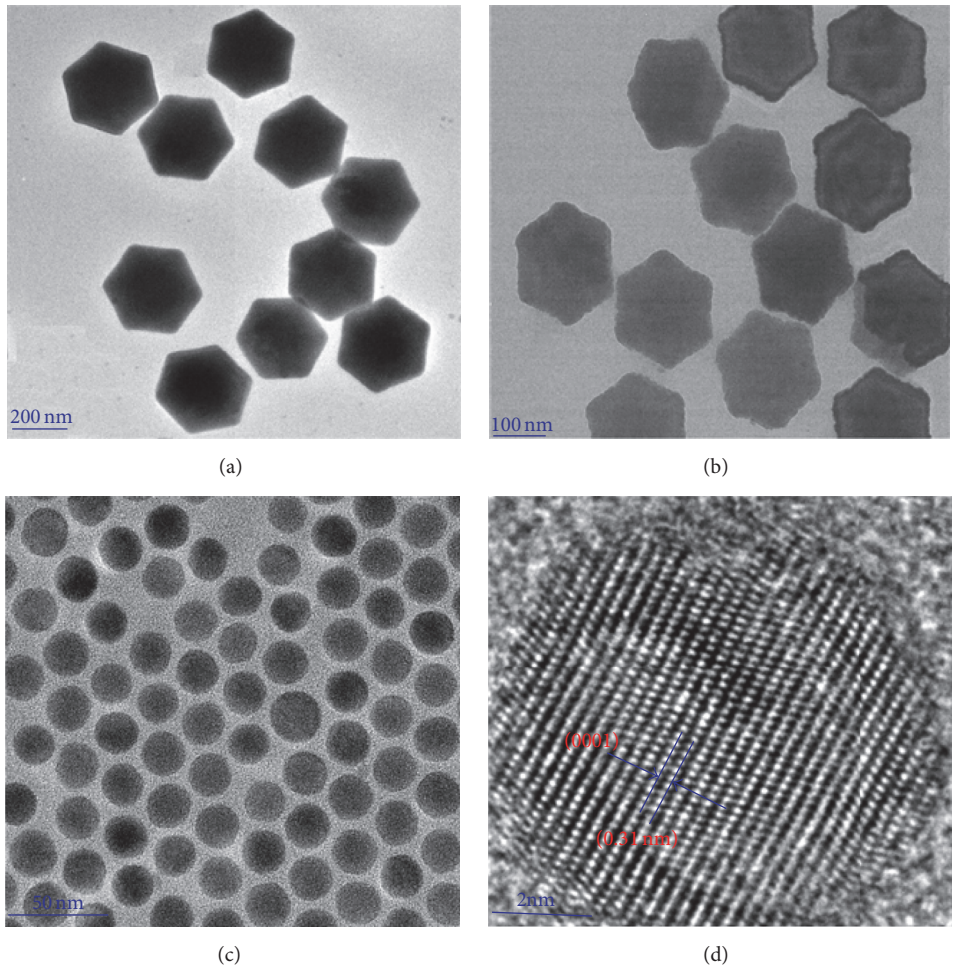

FIGURE 1: TEM images of upconversion nanocrystals: (a) $NaLuF_4$:20%Yb^{3+}/0.5%Tm^{3+}; (b) $NaLuF_4$:20%Yb^{3+}/0.5%Tm^{3+}/20%Gd^{3+}; (c) $NaLuF_4$:20%Yb^{3+}/0.5%Tm^{3+}/60%Gd^{3+}; $NaLuF_4$:20%Yb^{3+}/0.5%Tm^{3+}; (d) the high-resolution TEM image of (c).

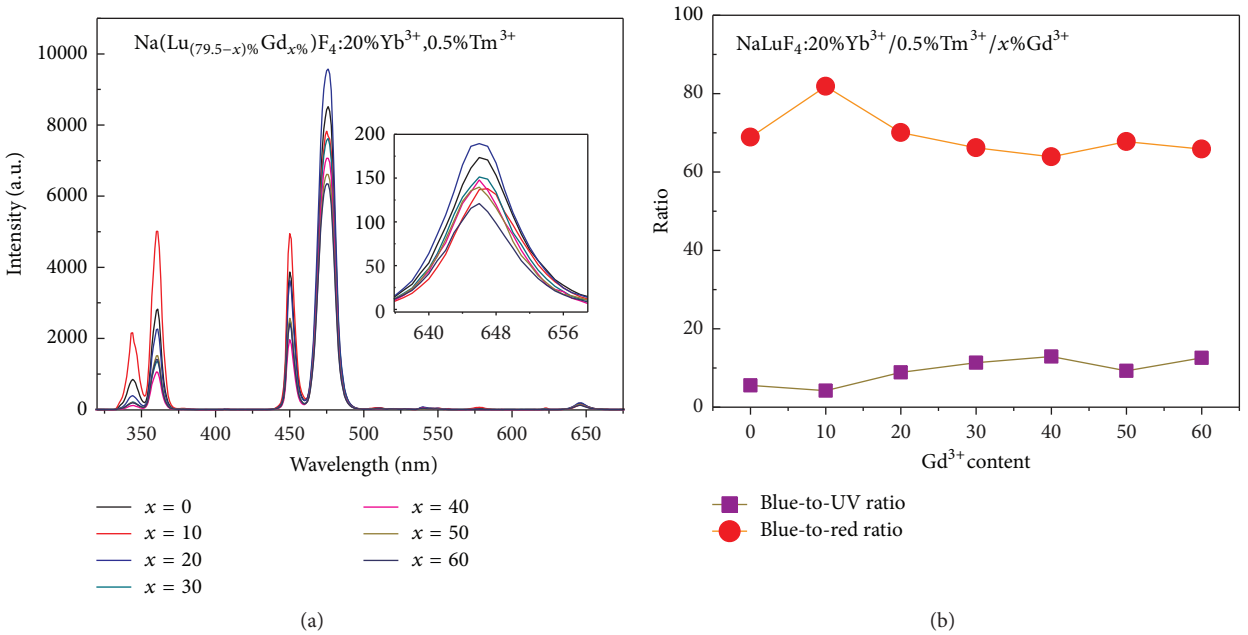

FIGURE 2: The upconversion luminescence emission properties: (a) relationships between the luminescent intensity of $NaLuF_4$:Yb^{3+}/Tm^{3+}/Gd^{3+} nanocrystals and the concentration of Gd^{3+}; (b) relationships between the Blue-to-UV and Blue-to-Red intensity ratios and the concentration of Gd^{3+}.

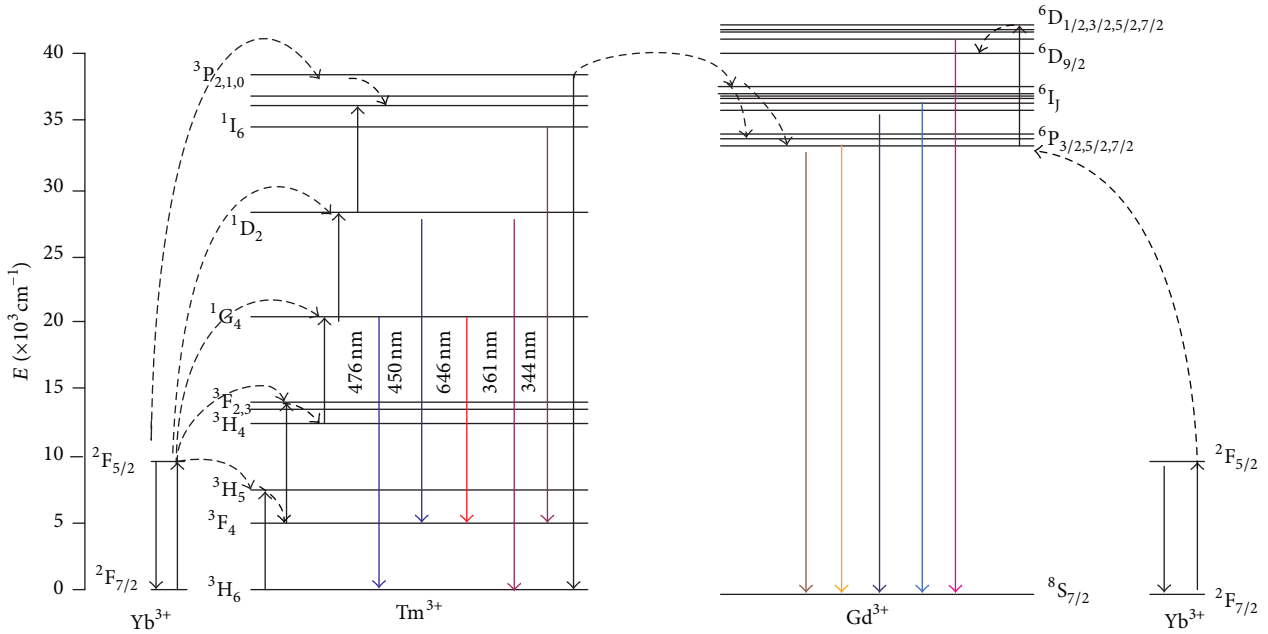

FIGURE 3: Scheme energy level diagrams of Yb^{3+}, Tm^{3+}, and Gd^{3+}, and possible UC processes in the samples.

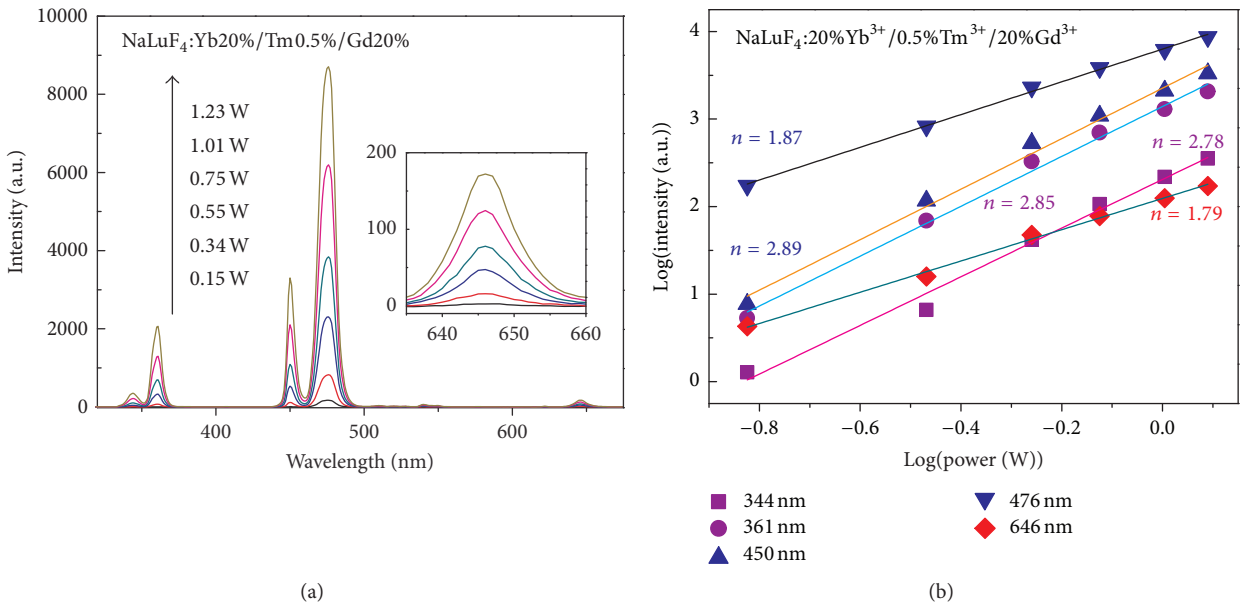

FIGURE 4: Relationships between the upconversion emissions of $NaLuF_4$:20%Yb^{3+}/0.5%Tm^{3+}/20%Gd^{3+} nanocrystals and the pump power density. (a) UC emission spectrum at different excitation powers; (b) log-log plot of the UC emission intensity versus the pump power density.

^6D_J levels because of the strong absorption of Yb^{3+} under 980 nm excitation and the high concentration of Yb^{3+} in the samples. UV and violet emissions also may be observed when transitions happen from the excited states ^6D_J, ^6I_J, ^6P_J levels of Gd^{3+}.

The pumping power dependence of the fluorescent intensity has been investigated. For an unsaturated UC process, the emission intensity is proportional to the power density of the excitation light, and the slope value (n) is the number of the excitation photons absorbed per emitted photon. The excitation power dependence of the five emission bands of $NaLuF_4$:20%Yb^{3+}/0.5%Tm^{3+}/20%Gd^{3+} nanocrystals is measured, and treated by Auzel's method (Figure 4(b)) [27]. Figure 4 shows the power dependence of the UC emission intensities: n = 2.78, 2.85, 2.89, 1.87, and 1.79 for 344, 361, 450, 476, and 646 nm emissions, respectively. Due to the saturation effect [28, 29], the n-values of all the five bands are much lower than the theoretical values. When the intermediate excited level has nearly saturated population, it

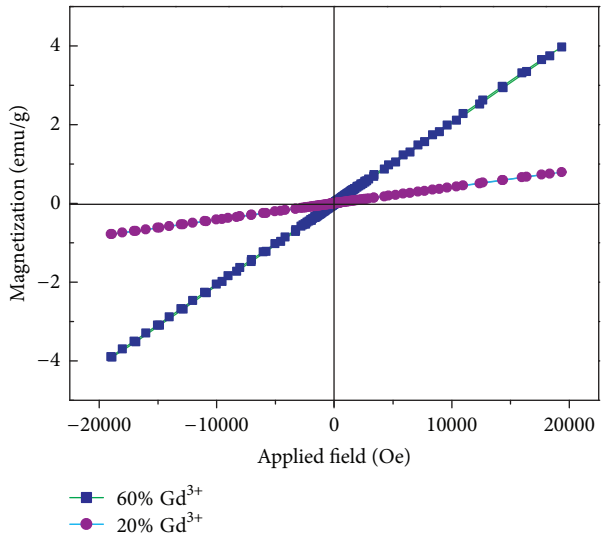

FIGURE 5: Relationships between the magnetization of $NaLuF_4$:Yb^{3+},Tm^{3+},Gd^{3+} nanocrystals and the applied magnetic field.

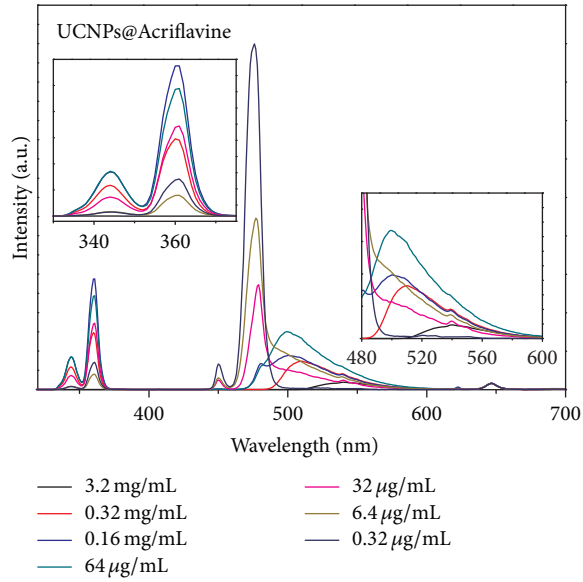

FIGURE 6: Evolution of the UC luminescence spectra of UCNPs@Acriflavine with different concentration of acriflavine at 0.34 W. Insert of Figure 6: the local amplification of the UCL spectra.

will act as electron reservoir like the ground state and directly transit electrons from its level to the upper one. As a result, it is observed that all the 344, 361, and 450 nm emissions came from three-photon UC processes and two-photon processes are related to the production of 476 and 646 nm emissions.

3.2. Magnetic Behavior. Besides the excellent luminescence characteristic, the Gd^{3+} doped $NaLuF_4$ nanocrystals also present particular magnetic properties due to the large magnetic moment of Gd^{3+}. Figure 5 shows the relationships between the magnetization of $NaLuF_4$ nanocrystals doped with different Gd^{3+} ions and the applied magnetic field (from −20 kOe to 20 kOe). It can be seen that both of the two samples present typical paramagnetic behavior, which is mainly because that the seven unpaired inner 4f electrons tightly bound to the nucleus and are effectively shielded by the outer closed shell electrons ($5s_2 5p_6$) from the crystal field. The paramagnetic properties of $NaLuF_4$ nanocrystals can be significantly modulated by doping Gd^{3+} ions. With the increasing of Gd^{3+} content, the magnetization is greatly improved. When the concentration of Gd^{3+} ions increased to 60%, under the applied magnetic field of 20000 Oe, the magnetization of the nanocrystals can reach to 3.9388 emu/g. If we continue to improve the doping concentration of Gd^{3+} ions, the magnetization of the nanocrystals will be further improved, but the overall intensity of the luminescence will decrease.

3.3. Detection of Acriflavine. Acriflavine is an organic material which is widely used in biochemical research and cell biology experiments. It can emit green light of ~540 nm under the excitation of 470 nm blue light and is preferably dissolved in water, methanol, and ethanol. Acriflavine is known as an antibacterial drug initially approved for the clinical treatment. Recently, increasing evidence has shown that acriflavine exhibits potential antitumor activity and has been recognized as an attractive molecule suitable for cancer chemotherapeutics. On the basis of effective monitoring of acriflavine, we can better explore its mechanism of action and broaden its scope of application in clinic.

The excitation spectra of acriflavine overlaps with the emission spectra of $NaLuF_4$:Yb^{3+},Tm^{3+},Gd^{3+} nanoparticles in blue region. Based on LRET, we can successfully build a sensor system, in which UCNPs play a role of energy donor while acriflavine plays a role of energy acceptor. The basic molecule acriflavine can be quickly captured by the acidic ligand (oleic acid) which lies in the synthesized UCNPs, so that a close nanosystem of UCNPs@Acriflavine is formed. By comparing the relative emission intensities of green emission (acriflavine) and blue emission (UCNPs with emitter Tm^{3+}), the concentration of acriflavine can be correspondingly determined. Here, we show that upconversion $NaLuF_4$:20%Yb^{3+}/0.5%Tm^{3+}/20%Gd^{3+} nanoprobes are very efficient and viable for detection of acriflavine.

The UC luminescence spectra of UCNPs@Acriflavine system with various concentrations of acriflavine are shown in Figure 6. With the increase of acriflavine concentration, blue emission intensity from the UCNP is reduced, while the emission of acriflavine centered at 490~540 nm becomes stronger gradually. It shows that the energy transfer between UCNP and acriflavine is enhanced with increasing the content of acriflavine. Interestingly, the variation of acriflavine concentration has no obvious influence on the emission of the red from Tm^{3+} ion. The exciton recombination radiation in acriflavine is highly dependent on LRET from UCNPs to acriflavine. When the concentration reaches 3.2 mg/mL, the blue and UV emission peak of UCNPs disappear while acriflavine shows intense emission centered at 540 nm. Similarly,

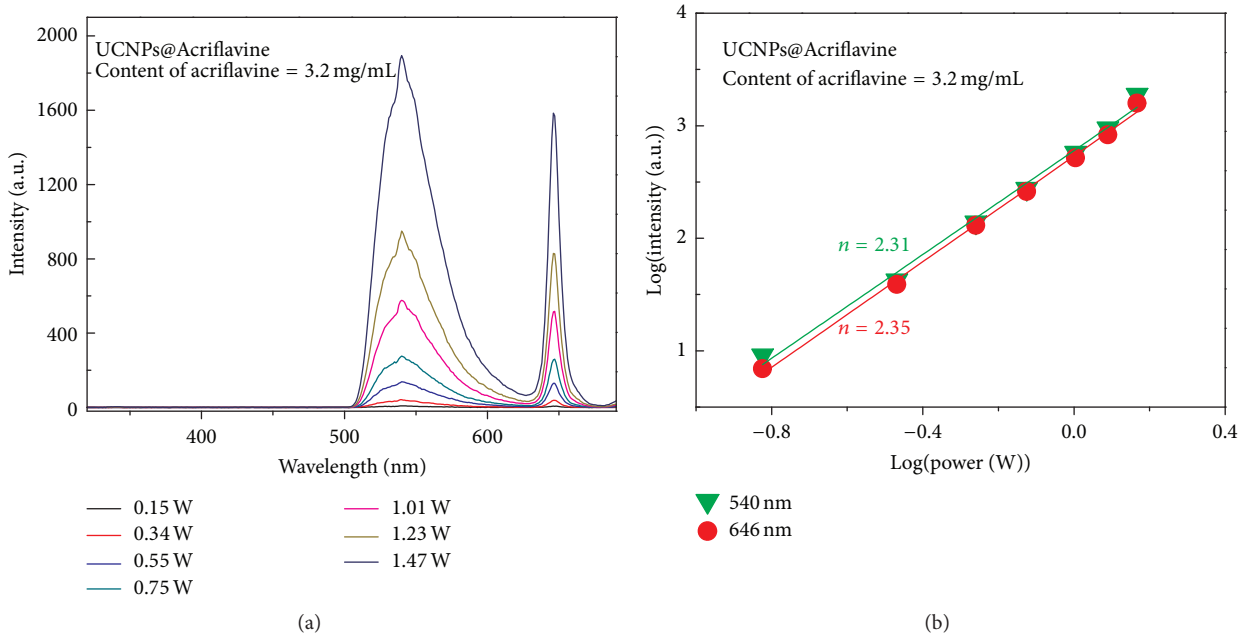

FIGURE 7: Power dependence of the UC emissions of UCNPs@Acriflavine system with the concentration of acriflavine at 3.2 mg/mL. (a) UC emission spectrum at different excitation powers; (b) log-log plot of emission intensity versus pump power density in UCNPs@ Acriflavine system.

it can be found that the integrated intensity ratio of green (acriflavine) to blue (UCNPs) emission (IIRGB) is strongly correlated with the concentration of acriflavine. The IIRGB is decreased with the decrease of acriflavine concentration. It is clear that this procedure based on LRET process is very efficient for detecting acriflavine in vitro. Figure 7 shows the pumping power dependence of the fluorescent intensity of UCNPs@Acriflavine system with the concentration of acriflavine fixed at 3.2 mg/mL. The slope values are equal to 2.31 and 2.35 for the observed acriflavine emission centered at 540 and UCNPs emission centered at 646 nm, respectively. This indicates that two-photon upconversion process is involved in both of acriflavine and UCNPs emissions. Using a 980 nm diode infrared power source of 0.34 W/mm^2, the acriflavine detection limit can reach 0.32 μg/mL, if properly controlling the concentration of upconversion nanoprobes.

Upconversion fluorescent spectra of UCNPs@Acriflavine with various concentrations of $NaLuF_4$:20%Yb^{3+}/0.5%Tm^{3+}/20%Gd^{3+} nanoparticles are shown in Figure 8. When the concentration of acriflavine is fixed at 0.32 mg/mL, four emission peaks, centered at 341 nm, 365 nm, 510 nm, and 646 nm, are also observed for this UCNPs@Acriflavine system which can be assigned to the electronic transitions $^1I_6 \rightarrow {}^3F_4$, $^1D_2 \rightarrow {}^3H_6$, and $^1G_4 \rightarrow {}^3F_4$ of Tm^{3+} ions and the emission of acriflavine, respectively. It is clear that both the green emission from acriflavine and blue emission from UCNPs increase with increasing the concentration of upconversion nanocrystals, which indicates that the LRET efficiency has no obvious change with increasing the concentration of upconversion nanocrystals. It can be inferred that the concentration of 25 mg/mL for UCNPs has not reached to the saturation value.

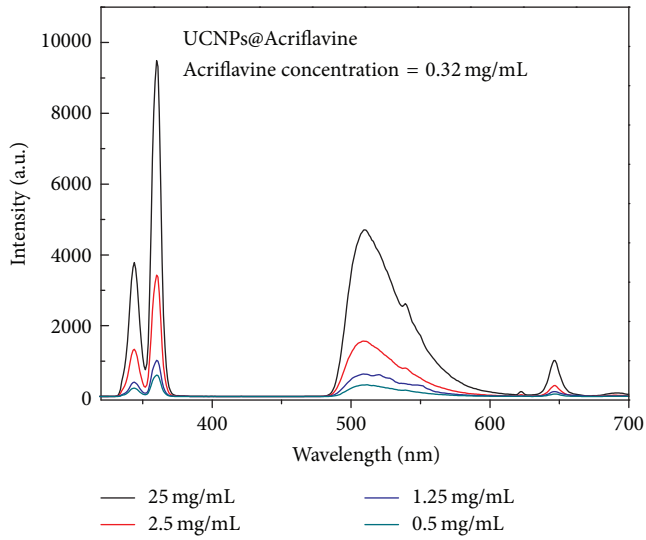

FIGURE 8: Evolution of the fluorescence spectra of UCNPs@Acriflavine in the case of different concentrations of UCNPs (from 0.5 to 20 mg/mL).

In addition, we used LRET tuned UCNPs for imaging tail fin tissues of crucian carp. The fluorescence imaging of tail fin tissues with UCNPs@Acriflavine under different excitation power is depicted in Figure 9, where the concentration of acriflavine is fixed at 0.32 mg/mL. It is clearly observed that the tail fin tissues exhibited bright cyan light, which is caused by the overlap of blue and green light. Increasing the excitation power, the luminous intensity is gradually enhanced, which indicates that the LRET from UCNPs to

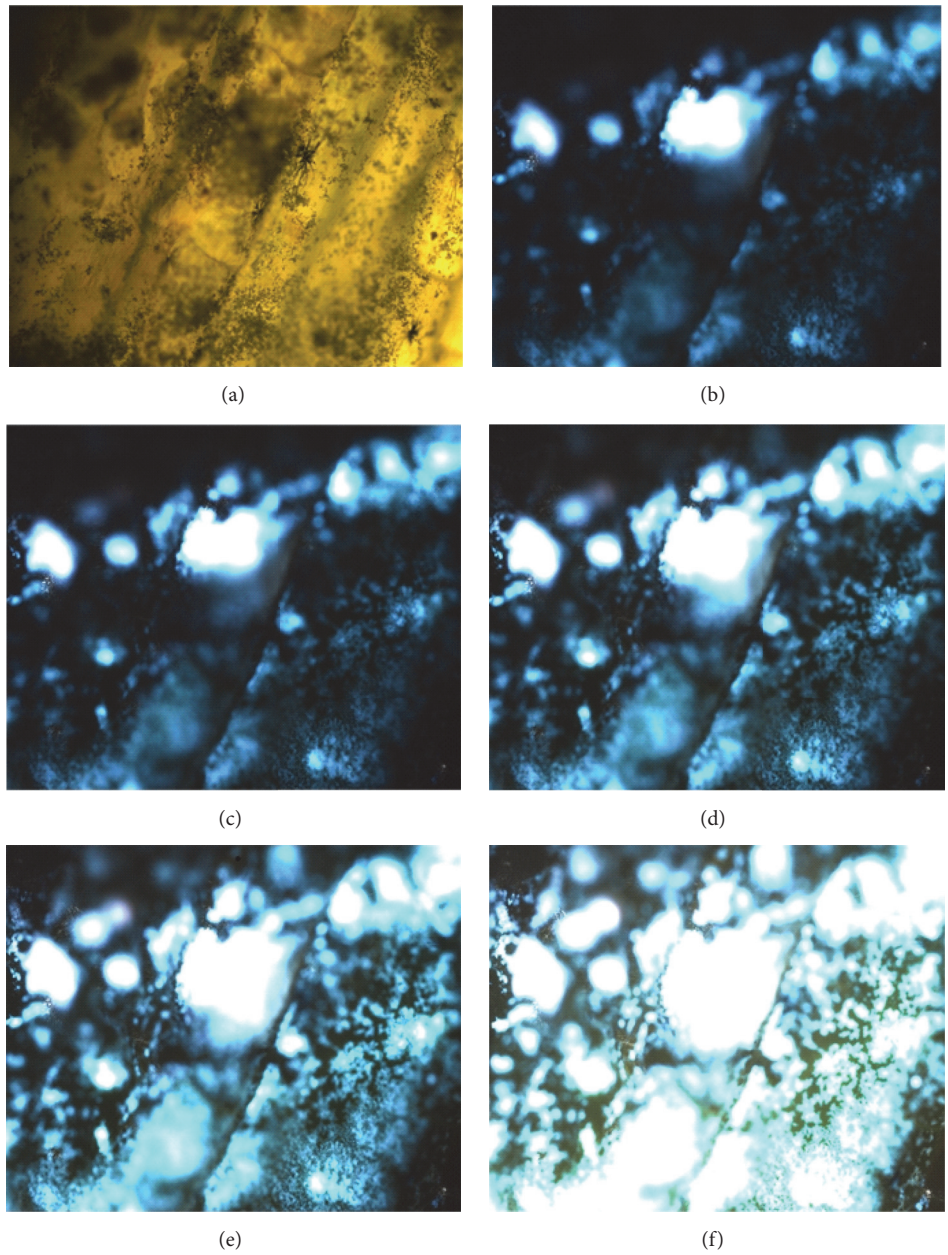

Figure 9: (a) Conventional slice transmission imaging; (b–f) fluorescence imaging of tail fin tissues of crucian carp with UCNPs@Acriflavine under different excitation power: (b) 0.15 W, (c) 0.2 W, (d) 0.3 W, (e) 0.34 W, and (f) 0.55 W.

acriflavine is remarkably raised with the increase of excitation power.

4. Conclusion

In conclusion, uniform $NaLuF_4$:Yb^{3+}/Tm^{3+}/Gd^{3+} nanocrystals were synthesized by the solvothermal method and subsequent surface modification. Doping with Gd^{3+} can easily modulate the particle size of these $NaLuF_4$ nanoparticles. Both the upconversion luminescence and magnetic property of $NaLuF_4$:Yb^{3+}/Tm^{3+}/Gd^{3+} can be adjusted by controlling the doping level of Gd^{3+}. The Gd^{3+} doped $NaLuF_4$ nanocrystals have good paramagnetic behavior at room temperature, which provides a simple strategy to merge the two functions into a single phase material. The as-synthesized upconversion nanoprobes have an acidic ligand which can quickly capture the basic dyes acriflavine to form a close UCNPs@Acriflavine system. After absorbing blue emission from $NaLuF_4$:20%Yb^{3+}/0.5%Tm^{3+}/20%Gd^{3+} by LRET, acriflavine can emit blue light. Based on the intensity ratio of blue to green emission, the detection limit of acriflavine for this upconversion fluorescent nanoprobe can reach up to 0.32 μg/mL. This novel route for detecting the acriflavine

molecules will be beneficial to explore its biological activity and broaden its clinic application.

Competing Interests

The authors declare that there is no conflict of interests regarding the publication of this paper.

Acknowledgments

This research was financially supported by the National Natural Science Foundation of China (Grant nos. 61376076, 61674056, 61675067, 61575062, and 61377024) and the Scientific Research Fund of Hunan Provincial Education Department (Grant nos. 16A072 and 16C0627).

References

[1] F. Wang, Y. Han, C. S. Lim et al., "Simultaneous phase and size control of upconversion nanocrystals through lanthanide doping," *Nature*, vol. 463, no. 7284, pp. 1061–1065, 2010.

[2] S. Hu, X. Wu, Z. Chen et al., "Uniform $NaLuF_4$ nanoparticles with strong upconversion luminescence for background-free imaging of plant cells and ultralow power detecting of trace organic dyes," *Materials Research Bulletin*, vol. 73, pp. 6–13, 2016.

[3] G. Y. Chen, H. L. Qiu, P. N. Prasad, and X. Y. Chen, "Upconversion nanoparticles: design, nanochemistry, and applications in theranostics," *Chemical Reviews*, vol. 114, no. 10, pp. 5161–5214, 2014.

[4] S. Zeng, M.-K. Tsang, C.-F. Chan, K.-L. Wong, and J. Hao, "PEG modified BaGdF5: Yb/Er nanoprobes for multi-modal upconversion fluorescent, in vivo X-ray computed tomography and biomagnetic imaging," *Biomaterials*, vol. 33, no. 36, pp. 9232–9238, 2012.

[5] Z. Chen, X. Wu, S. Hu et al., "Upconversion $NaLuF_4$ fluorescent nanoprobes for jellyfish cell imaging and irritation assessment of organic dyes," *Journal of Materials Chemistry C*, vol. 3, no. 23, pp. 6067–6076, 2015.

[6] S. Hu, X. Wu, Z. Tang et al., "Upconversion $NaYF_4$ nanoparticles for size dependent cell imaging and concentration dependent detection of rhodamine B," *Journal of Nanomaterials*, vol. 2015, Article ID 598734, 10 pages, 2015.

[7] X. Wu, P. Hu, S. Hu et al., "Upconversion nanoparticles for differential imaging of plant cells and detection of fluorescent dyes," *Journal of Rare Earths*, vol. 34, no. 2, pp. 208–220, 2016.

[8] Y. Liu, D. Wang, L. Li, Q. Peng, and Y. Li, "Energy upconversion in lanthanide-doped core/porous-shell nanoparticles," *Inorganic Chemistry*, vol. 53, no. 7, pp. 3257–3259, 2014.

[9] M.-K. Tsang, C.-F. Chan, K.-L. Wong, and J. Hao, "Comparative studies of upconversion luminescence characteristics and cell bioimaging based on one-step synthesized upconversion nanoparticles capped with different functional groups," *Journal of Luminescence*, vol. 157, pp. 172–178, 2015.

[10] G. Tian, X. Zhang, Z. Gu, and Y. Zhao, "Recent advances in upconversion nanoparticles-based multifunctional nanocomposites for combined cancer therapy," *Advanced Materials*, vol. 27, no. 47, pp. 7692–7712, 2015.

[11] Z. Chen, X. Wu, S. Hu et al., "Multicolor upconversion NaLuF4 fluorescent nanoprobe for plant cell imaging and detection of sodium fluorescein," *Journal of Materials Chemistry C*, vol. 3, no. 1, pp. 153–161, 2015.

[12] Z. Yi, X. Li, Z. Xue et al., "Remarkable NIR enhancement of multifunctional nanoprobes for in vivo trimodal bioimaging and upconversion optical/T2−weighted MRI−guided small tumor diagnosis," *Advanced Functional Materials*, vol. 25, no. 46, pp. 7119–7129, 2015.

[13] S. Zeng, H. Wang, W. Lu et al., "Dual-modal upconversion fluorescent/X-ray imaging using ligand-free hexagonal phase $NaLuF_4$: Gd/Yb/Er nanorods for blood vessel visualization," *Biomaterials*, vol. 35, no. 9, pp. 2934–2941, 2014.

[14] S. Hu, Y. Liu, X. Wu et al., "Remarkable red-shift of upconversion luminescence and anti-ferromagnetic coupling in $NaLuF_4$:Yb^{3+}/Tm^{3+}/Gd^{3+}/Sm^{3+} bifunctional microcrystals," *Journal of Rare Earths*, vol. 34, no. 2, pp. 166–173, 2016.

[15] S. Zeng, J. Xiao, Q. Yang, and J. Hao, "Bi-functional $NaLuF_4$:Gd^{3+}/Yb^{3+}/Tm^{3+} nanocrystals: structure controlled synthesis, near-infrared upconversion emission and tunable magnetic properties," *Journal of Materials Chemistry*, vol. 22, no. 19, pp. 9870–9874, 2012.

[16] J. L. Mueller, H. L. Fu, J. K. Mito et al., "A quantitative microscopic approach to predict local recurrence based on in vivo intraoperative imaging of sarcoma tumor margins," *International Journal of Cancer*, vol. 137, no. 10, pp. 2403–2412, 2015.

[17] H. K. Can, G. Karakus, and N. Tuzcu, "Synthesis, characterization and in vitro antibacterial assessments of a novel modified poly[maleic anhydride-alt-acrylic acid]/acriflavine conjugate," *Polymer Bulletin*, vol. 71, no. 11, pp. 2903–2921, 2014.

[18] L. Zhang, B. Liu, Z. Li, and Y. Guo, "Comparative studies on the interaction of cefixime with bovine serum albumin by fluorescence quenching spectroscopy and synchronous fluorescence spectroscopy," *Luminescence*, vol. 30, no. 5, pp. 686–692, 2015.

[19] Z. Li, S. Lv, Y. Wang, S. Chen, and Z. Liu, "Construction of LRET-based nanoprobe using upconversion nanoparticles with confined emitters and bared surface as luminophore," *Journal of the American Chemical Society*, vol. 137, no. 9, pp. 3421–3427, 2015.

[20] S. Dai, S. Wu, N. Duan, and Z. Wang, "A luminescence resonance energy transfer based aptasensor for the mycotoxin Ochratoxin A using upconversion nanoparticles and gold nanorods," *Microchimica Acta*, vol. 183, no. 6, pp. 1909–1916, 2016.

[21] S. Zhao, F. Wu, Y. Zhao, Y. Liu, and L. Zhu, "Phenothiazine-cyanine-functionalized upconversion nanoparticles for LRET and colorimetric sensing of cyanide ions in water samples," *Journal of Photochemistry and Photobiology A: Chemistry*, vol. 319-320, pp. 53–61, 2016.

[22] E. J. Jo, H. Mun, and M. G. Kim, "Homogeneous immunosensor based on luminescence resonance energy transfer for glycated hemoglobin detection using upconversion nanoparticles," *Analytical Chemistry*, vol. 88, no. 5, pp. 2742–2746, 2016.

[23] J. Liu, J. Cheng, and Y. Zhang, "Upconversion nanoparticle based LRET system for sensitive detection of MRSA DNA sequence," *Biosensors and Bioelectronics*, vol. 43, no. 1, pp. 252–256, 2013.

[24] L. Zhao, J. Peng, M. Chen et al., "Yolk-shell upconversion nanocomposites for LRET sensing of cysteine/homocysteine," *ACS Applied Materials and Interfaces*, vol. 6, no. 14, pp. 11190–11197, 2014.

[25] C. Cao, W. Qin, J. Zhang et al., "Ultraviolet upconversion emissions of Gd^{3+}," *Optics Letters*, vol. 33, no. 8, pp. 857–859, 2008.

[26] J. Sytsma, G. F. Imbusch, and G. Blasse, "The decay of the $^6I_{7/2}$ term level of Gd^{3+} in YOCl and $LiYF_4$," *Journal of Physics: Condensed Matter*, vol. 2, no. 23, article 5171, 1990.

[27] F. E. Auzel, "Materials and devices using double-pumped-phosphors with energy transfer," *Proceedings of the IEEE*, vol. 61, no. 6, pp. 758–786, 1973.

[28] F. Pandozzi, F. Vetrone, J.-C. Boyer et al., "A spectroscopic analysis of blue and ultraviolet upconverted emissions from $Gd_3Ga_5O_{12}$:Tm^{3+}, Yb^{3+} nanocrystals," *The Journal of Physical Chemistry B*, vol. 109, no. 37, pp. 17400–17405, 2005.

[29] H. Sun, Z. Duan, G. Zhou et al., "Structural and up-conversion luminescence properties in Tm^{3+}/Yb^{3+}-codoped heavy metal oxide-halide glasses," *Spectrochimica Acta—Part A: Molecular and Biomolecular Spectroscopy*, vol. 63, no. 1, pp. 149–153, 2006.